The 8th European Congress on Computational Methods in Applied Sciences and Engineering
ECCOMAS Congress 2022
5-9 June 2022, Oslo, Norway

EFFICIENT ASSESSMENT OF NOISE TRANSMISSION THROUGH HIGHLY FLEXIBLE SLENDER STRUCTURES

FABIO SCHNEIDER-JUNG[1], LILLI BURGER[1] AND JOACHIM LINN[1]

[1] Fraunhofer Institute for Industrial Mathematics
Fraunhofer-Platz 1, 67663 Kaiserslautern
e-mail: fabio.julian.schneider-jung@itwm.fraunhofer.de

Key words: Cosserat Rod, Mechanical Impedance

Abstract. In this work, we propose an efficient methodology for the assessment of noise transmission through cables and hoses. An interactive simulation with a geometrically exact Cosserat rod enables simple and fast modelling of various configurations. Subsequently, we linearise the equations of motion at the static equilibrium for given boundary conditions and, using the resulting system matrices, compute the mechanical impedance matrix. The computation result, i.e. the impedance matrix, is available within seconds.

The impedance matrix either can be used to compute reaction forces for given excitation or, if the excitation is unknown, allows to analyse the transmission of noise by looking at single matrix elements. The latter is especially useful in early, purely virtual development phases.

1 INTRODUCTION

Modern vehicles are full of cables and hoses. Kilometres of wiring harness can be found e.g. in doors, seats, the axle or on the engine. Also hoses perform important functions and are therefore numerous in the vehicle. Apparently, the development of battery-electric vehicles requires new assembly concepts, e.g. for cooling hoses, or even new components like high-voltage cables. In both cases, well known assembly concepts typically are not applicable or simply unknown. Therefore, an interactive assembly simulation of cables and hoses is very helpful and widely used in vehicle development [1, 2]. The simulation utilizes a geometrically non-linear rod model as presented in [3, 4].

In this work, we focus on the topic of noise transmission through cables and hoses. In practice, cables and hoses may transmit undesired noise into the vehicle cabin. To assess this noise transmission already in early design phases of the vehicle development, we suggest an efficient and simple methodology: linearise a geometrically exact rod at its static equilibrium and compute the mechanical impedance.

The interactive rod simulation as described in [3] allows an easy and comfortable generation of configuration variants, e.g. a cable with different boundary conditions or a hose with an alternative stress-free shape (see Figure 1). In general, an assembled cable or hose, i.e. the static equilibrium of a rod under given boundary conditions, is pre-stressed and undergoes large deformations, such that a geometrically non-linear rod model is essential. Nevertheless, to compute the mechanical impedance matrix, a linearised version of the rod's equations of motion is required. This is achieved by applying algorithmic differentiation to the non-linear

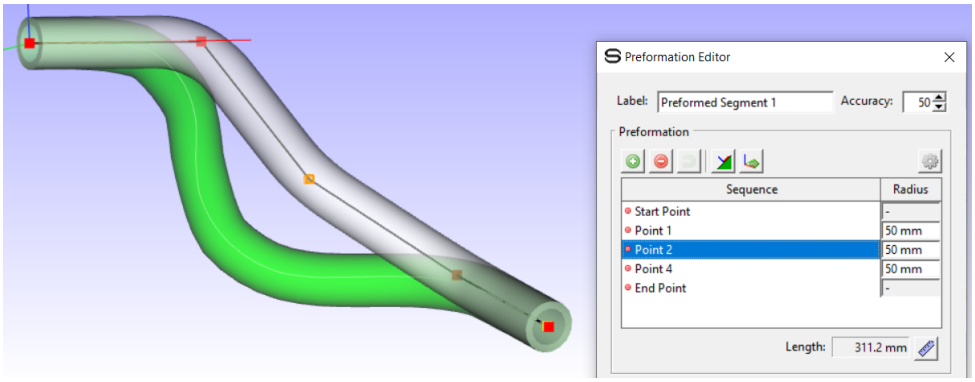

Figure 1: Interactive manipulation of the stress-free hose shape in *IPS Cable Simulation* [2].

equations of motion. Finally, the mechanical impedance matrix is computed from the linear system matrices and one can investigate the noise transmission. The entire computation only takes seconds, such that many variants can easily be analysed and compared.
If a concrete excitation vector is known, the impedance matrix allows to compute reaction forces at the rod's boundaries. However, often the excitation vector might be unknown, e.g., in early development phases. In this case, one can analyse single elements of the impedance matrix, each describing how vibrations are transmitted from a certain boundary degree of freedom to another boundary degree of freedom.

The paper is structured as follows: In Section 2 we describe a geometrically exact Cosserat rod and its non-linear equations of motion. After that, in Section 3, we discuss their linearised version. Section 4 shows how to compute the mechanical impedance. Finally, an application example is presented in Section 5, before we give some concluding remarks in Section 6.

2 GEOMETRICALLY EXACT COSSERAT ROD

Our starting point is the geometrically exact Cosserat rod as given in [3, 4]. It allows a real-time capable user interaction and, thus, enables interactive modifications of the rod, either by changing its preformed shape (i.e. its stress-free configuration) or by manipulating the rod connectors (i.e. its boundary conditions).

We first will introduce the continuous Cosserat rod. After that, we focus on its discrete counterpart and present the corresponding equations of motion.

2.1 Continuous Cosserat rod

The continuous version of the rod with length L and simulation time T is described with a centreline

$$\boldsymbol{x}: \ [0,L] \times [0,T] \ \to \mathbb{R}^3, \qquad (s,t) \mapsto \boldsymbol{x}(s,t) \tag{1}$$

and the orientation frame

$$\boldsymbol{R} \circ \boldsymbol{p}: \ [0,L] \times [0,T] \ \to SO(3), \qquad (s,t) \mapsto \boldsymbol{R}(\boldsymbol{p}(s,t)). \tag{2}$$

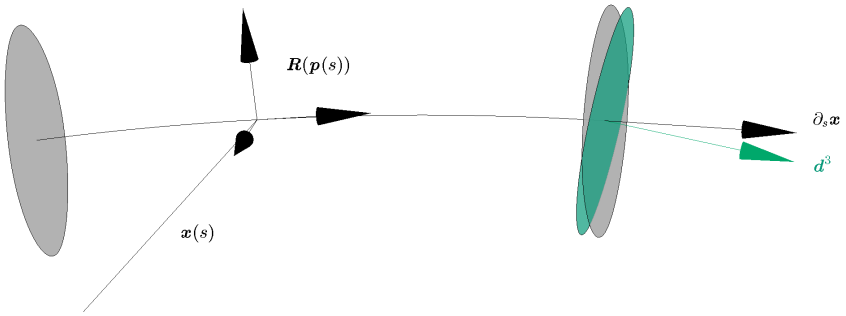

Figure 2: Continuous Cosserat rod with centreline $\boldsymbol{x}(s)$ and moving frame $\boldsymbol{R}(\boldsymbol{p}(s))$.

Here, the rotation is parametrized by unit quaternions ($\|\boldsymbol{p}\| = 1$)

$$\boldsymbol{p}: \ [0, L] \times [0, T] \ \to \mathbb{S}^3 \subset \mathbb{R}^4, \qquad (s, t) \mapsto \boldsymbol{p}(s, t) \tag{3}$$

which can be written as

$$\boldsymbol{p} = p_s + p_x i + p_y j + p_z k \tag{4}$$

with basis vectors given as the standard basis $i = \boldsymbol{e}^1$, $j = \boldsymbol{e}^2$ and $k = \boldsymbol{e}^3$. Every quaternion $\boldsymbol{p}$ has a conjugate quaternion $\bar{\boldsymbol{p}} = p_s - \hat{\boldsymbol{p}}$, where we abbreviate the imaginary part of the quaternion by $\hat{\boldsymbol{p}} := p_x i + p_y j + p_z k$. For two quaternions $\boldsymbol{p}$ and $\boldsymbol{q}$, the sum is simply given as

$$\boldsymbol{p} + \boldsymbol{q} := (p_s + q_s) + (p_x + q_x)i + (p_y + q_y)j + (p_z + q_z)k, \tag{5}$$

while the quaternion product is defined as

$$\boldsymbol{pq} := p_s q_s - \langle \hat{\boldsymbol{p}}, \hat{\boldsymbol{q}} \rangle + p_s \hat{\boldsymbol{q}} + q_s \hat{\boldsymbol{p}} + \hat{\boldsymbol{p}} \times \hat{\boldsymbol{q}}. \tag{6}$$

The quaternion product can also be written as matrix vector multiplication. For that purpose, we define the quaternion matrix

$$\boldsymbol{Q}(\boldsymbol{p}) := \begin{pmatrix} p_s & -p_x & -p_y & -p_z \\ p_x & p_s & -p_z & p_y \\ p_y & p_z & p_s & -p_x \\ p_z & -p_y & p_x & p_s \end{pmatrix}, \tag{7}$$

such that it holds $\boldsymbol{pq} = \mathcal{Q}(\boldsymbol{p})\boldsymbol{q}$ and $\bar{\boldsymbol{p}}\boldsymbol{q} = \mathcal{Q}(\boldsymbol{p})^T \boldsymbol{q}$.
The Euler map $\boldsymbol{R}: \mathbb{S}^3 \setminus \{\pm 1\} \to SO(3), \ \ \boldsymbol{p} \mapsto \boldsymbol{R}(\boldsymbol{p})$ maps unit quaternions on rotation matrices

$$\boldsymbol{R}(\boldsymbol{p}) = \begin{pmatrix} p_s^2 + p_x^2 - p_y^2 - p_z^2 & 2(p_x p_y - p_s p_z) & 2(p_x p_z + p_s p_y) \\ 2(p_x p_y + p_s p_z) & p_s^2 - p_x^2 + p_y^2 - p_z^2 & 2(p_y p_z - p_s p_x) \\ 2(p_x p_z - p_s p_y) & 2(p_y p_z + p_s p_x) & p_s^2 - p_x^2 - p_y^2 + p_z^2 \end{pmatrix}. \tag{8}$$

It holds $\boldsymbol{R}(\boldsymbol{pq}) = \boldsymbol{R}(\boldsymbol{p})\boldsymbol{R}(\boldsymbol{q})$, $\boldsymbol{R}(\bar{\boldsymbol{p}}) = \boldsymbol{R}(\boldsymbol{p})^T$ and $\boldsymbol{R}(-\boldsymbol{p}) = \boldsymbol{R}(\boldsymbol{p})$. Moreover, for a purely imaginary quaternion, i.e. a vector $\boldsymbol{z} \in \mathbb{R}^3$, we have $\boldsymbol{R}(\boldsymbol{p})\boldsymbol{z} = \boldsymbol{pz}\bar{\boldsymbol{p}}$, where the multiplication has to be understood as quaternion product with $\left[0, \ \boldsymbol{z}^T\right]^T$.

The curvature vector and shear-extensional strain vector, are given as

$$\boldsymbol{K} = 2\bar{\boldsymbol{p}}\partial_s \boldsymbol{p} \qquad \text{and} \qquad \boldsymbol{\Gamma} = \bar{\boldsymbol{p}}\partial_s \boldsymbol{x}\boldsymbol{p} - \boldsymbol{e}^3. \tag{9}$$

The preformed shape of the rod is given by a pre-curvature vector $\boldsymbol{K}^0$ and we define $\Delta\boldsymbol{K} := \boldsymbol{K} - \boldsymbol{K}^0$. The elastic potential energy can be formulated as

$$\mathcal{V} = \frac{1}{2}\int_0^L \underbrace{\boldsymbol{\Gamma}^T\boldsymbol{C}^\Gamma\boldsymbol{\Gamma}}_{\text{shearing \& extension}} + \underbrace{\Delta\boldsymbol{K}^T\boldsymbol{C}^K\Delta\boldsymbol{K}}_{\text{bending \& torsion}}\, ds \tag{10}$$

with coefficient matrices containing the effective stiffness parameters

$$\boldsymbol{C}^\Gamma = \begin{pmatrix} [GA_1] & & \\ & [GA_2] & \\ & & [EA] \end{pmatrix} \quad \text{and} \quad \boldsymbol{C}^K = \begin{pmatrix} [EI_1] & & \\ & [EI_2] & \\ & & [GJ] \end{pmatrix}. \tag{11}$$

Those parameters combine material quantities (Young's modulus E and shear modulus G) and geometrical quantities (cross section area A, shear corrected cross section areas A_1 and A_2, geometric cross section moments of inertia I_1 and I_2 and the polar moment J) and, thus, formally depend on each other. However, for practical applications it is beneficial to consider the effective stiffness parameters as independent compound parameters. The notation within brackets $[\cdot]$ shall emphasize this fact.

Similar to the elastic potential energy, the dissipative energy $\mathcal{D}$ can be formulated with curvature and strain rates $\dot{\boldsymbol{K}}$ and $\dot{\boldsymbol{\Gamma}}$

$$\mathcal{D} = \frac{1}{2}\int_0^L \dot{\boldsymbol{\Gamma}}^T \begin{pmatrix} [\eta_G A_1] & & \\ & [\eta_G A_2] & \\ & & [\eta_E A] \end{pmatrix} \dot{\boldsymbol{\Gamma}} + \dot{\boldsymbol{K}}^T \begin{pmatrix} [\eta_E I_1] & & \\ & [\eta_E I_2] & \\ & & [\eta_G J] \end{pmatrix} \dot{\boldsymbol{K}}\, ds. \tag{12}$$

Again, the effective damping parameters are considered as independent compound parameters, although depending on each other via η_E and η_G.

The above dissipative energy implies a Kelvin-Voigt type damping. Although coming with some potential drawbacks, our approach has shown to be practically useful for transient dynamic simulations (see [5] for more details). One main advantage is that one can adjust stiffness parameters and damping parameters individually. If the Kelvin-Voigt type damping is also beneficial for the assessment of noise transmission, is not yet qualified. However, it will an optional damping approach, as we will see later in Section 4.

Finally, the kinetic energy is given as

$$\mathcal{T} = \underbrace{\frac{\varrho A}{2}\int_0^L \|\dot{\boldsymbol{x}}\| ds}_{\text{translatory}} + \underbrace{\frac{\varrho}{2}\int_0^L \boldsymbol{\omega}^T\boldsymbol{I}\boldsymbol{\omega} ds}_{\text{rotatory}}, \tag{13}$$

where ϱ is the density. The inertia tensor $\boldsymbol{I}$ is diagonal and contains I_1, I_2 and J as diagonal elements.

In principle, now one can derive equations of motion by applying the Lagrangian formalism. For more details, we refer to [4]. In this paper, we only present equations of motion for the discrete rod.

2.2 Discrete Cosserat rod

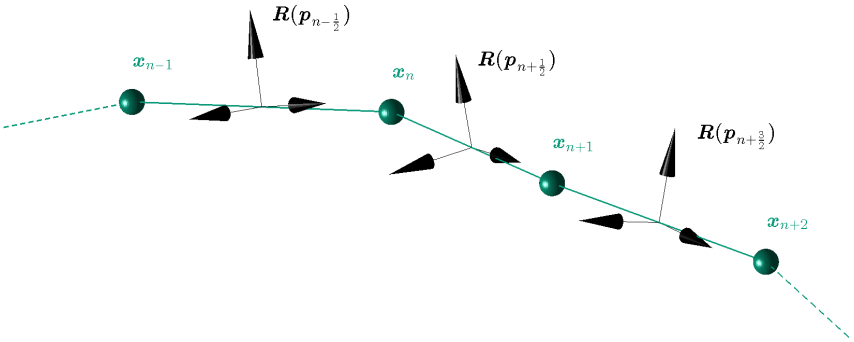

Figure 3: Discrete Cosserat rod with staggered grid: positions $\boldsymbol{x}_n$ in the nodes, unit quaternions $\boldsymbol{p}_{n-\frac{1}{2}}$ on the edges.

For the spatially discrete Cosserat rod, a staggered grid is used (see Figure 3) with translatory degrees of freedom

$$\boldsymbol{x}_0,\ \boldsymbol{x}_1,\ \ldots,\ \boldsymbol{x}_N \in \mathbb{R}^3 \tag{14}$$

situated in the $N+1$ nodes and rotatory degrees of freedom, here: unit quaternions,

$$\boldsymbol{p}_{\frac{1}{2}},\ \boldsymbol{p}_{1+\frac{1}{2}},\ \ldots,\ \boldsymbol{p}_{N-\frac{1}{2}} \in \mathbb{S}^3 \tag{15}$$

on the N edge midpoints. The edge length is defined as $\Delta s_{n-\frac{1}{2}} := s_n - s_{n-1}$. Moreover, we define $\delta s_n := \frac{1}{2}\left(\Delta s_{n+\frac{1}{2}} + \Delta s_{n-\frac{1}{2}}\right)$ for $n = 1, ..., N-1$ and $\delta s_0 := \frac{1}{2}\Delta s_{\frac{1}{2}}$ as well as $\delta s_N := \frac{1}{2}\Delta s_{N-\frac{1}{2}}$.

The discrete versions of shear-extensional strain vectors $\boldsymbol{\Gamma}_{n-\frac{1}{2}}$, situated on edges, and curvature vectors $\boldsymbol{K}_n$ (and pre-curvatures $\boldsymbol{K}_n^0$, such that $\Delta\boldsymbol{K}_n := \boldsymbol{K}_n - \boldsymbol{K}_n^0$), situated at the nodes, allow to formulate the discrete elastic potential energy as

$$\mathcal{V} = \underbrace{\frac{1}{2}\sum_{n=1}^{N} \Delta s_{n-\frac{1}{2}} \boldsymbol{\Gamma}^T_{n-\frac{1}{2}} \boldsymbol{C}^{\Gamma} \boldsymbol{\Gamma}_{n-\frac{1}{2}}}_{\text{shearing \& extension}} + \underbrace{\frac{1}{2}\sum_{n=0}^{N} \delta s_n \Delta\boldsymbol{K}_n^T \boldsymbol{C}^K \Delta\boldsymbol{K}_n}_{\text{bending \& torsion}}, \tag{16}$$

while strain and curvature rates are used to write the discrete dissipative energy

$$\mathcal{D} = \frac{1}{2}\sum_{n=1}^{N} \Delta s_{n-\frac{1}{2}} \dot{\boldsymbol{\Gamma}}^T_{n-\frac{1}{2}} \boldsymbol{C}^{\dot{\Gamma}} \dot{\boldsymbol{\Gamma}}_{n-\frac{1}{2}} + \frac{1}{2}\sum_{n=0}^{N} \delta s_n \dot{\boldsymbol{K}}_n^T \boldsymbol{C}^{\dot{K}} \dot{\boldsymbol{K}}_n. \tag{17}$$

The discrete kinetic energy is given as

$$\mathcal{T} = \underbrace{\frac{\varrho A}{2}\sum_{n=0}^{N} \delta s_n \|\dot{\boldsymbol{x}}_n\|^2}_{\text{translatory}} + \underbrace{\frac{\varrho}{2}\sum_{n=1}^{N} \Delta s_{n-\frac{1}{2}} \dot{\boldsymbol{p}}^T_{n-\frac{1}{2}} \left(4\boldsymbol{Q}(\boldsymbol{p}_{n-\frac{1}{2}})\boldsymbol{I}\boldsymbol{Q}(\boldsymbol{p}_{n-\frac{1}{2}})^T\right) \dot{\boldsymbol{p}}_{n-\frac{1}{2}}}_{\text{rotatory}}. \tag{18}$$

Here, we rewrite the material angular velocity in terms of quaternions as $\boldsymbol{\omega}_{n-\frac{1}{2}} = 2\bar{\boldsymbol{p}}_{n-\frac{1}{2}}\dot{\boldsymbol{p}}_{n-\frac{1}{2}}$ and used the quaternion matrix $\boldsymbol{Q}(p)$ to represent the quaternion multiplication.
Equations (16), (17) and (18) are discrete approximations of (10), (12) and (13), utilizing suitable quadrature rules. A detailed presentation can be found in [4].

The corresponding semi-discrete equations of motion are given by the Euler-Lagrange equations with the Lagrangian $\mathcal{L} = \mathcal{T} - \mathcal{V} - \mathcal{D}$. For the translatory degrees of freedom, we get

$$m_n\ddot{\boldsymbol{x}}_n = -\frac{\partial\mathcal{V}}{\partial\boldsymbol{x}_n} - \frac{\partial\mathcal{D}}{\partial\dot{\boldsymbol{x}}_n} + \boldsymbol{F}_n^x(t) =: \boldsymbol{f}_n^x \quad \text{for} \quad n = 0, 1, \ldots, N \tag{19}$$

with scalar mass $m_n = \varrho A\delta s_n$ and external force $\boldsymbol{F}_n^x(t)$. For the rotatory degrees of freedom, we end up with a system of differential-algebraic equations

$$\begin{aligned} \boldsymbol{M}(\boldsymbol{p}_{n-\frac{1}{2}})\ddot{\boldsymbol{p}}_{n-\frac{1}{2}} &= \boldsymbol{f}^p_{n-\frac{1}{2}} - \boldsymbol{p}_{n-\frac{1}{2}}\boldsymbol{\lambda}_{n-\frac{1}{2}} \\ 0 &= \tfrac{1}{2}(\|\boldsymbol{p}_{n-\frac{1}{2}}\|^2 - 1) \end{aligned} \qquad \text{for} \quad n = 1, 2, \ldots, N \tag{20}$$

with quaternion mass matrix $\boldsymbol{M}(\boldsymbol{p}_{n-\frac{1}{2}}) = 4\varrho\Delta s_{n-\frac{1}{2}}\boldsymbol{Q}(\boldsymbol{p}_{n-\frac{1}{2}})\boldsymbol{I}\boldsymbol{Q}(\boldsymbol{p}_{n-\frac{1}{2}})^T$. On the right hand side, it holds $\boldsymbol{f}^p_{n-\frac{1}{2}} := -\frac{\partial\mathcal{V}}{\partial\boldsymbol{p}_{n-\frac{1}{2}}} - \frac{\partial\mathcal{D}}{\partial\dot{\boldsymbol{p}}_{n-\frac{1}{2}}} + \frac{\partial\mathcal{T}}{\partial\boldsymbol{p}_{n-\frac{1}{2}}} - \frac{\partial}{\partial\boldsymbol{p}_{n-\frac{1}{2}}}\left(\boldsymbol{M}(\boldsymbol{p}_{n-\frac{1}{2}})\dot{\boldsymbol{p}}_{n-\frac{1}{2}}\right)\dot{\boldsymbol{p}}_{n-\frac{1}{2}} + \boldsymbol{F}^p_{n-\frac{1}{2}}(t)$ with external quaternion moments $\boldsymbol{F}^p_{n-\frac{1}{2}}(t)$. The gradient of the unit quaternion constraint is $\boldsymbol{p}^T_{n-\frac{1}{2}}$ and leads to constraint forces $-\boldsymbol{p}_{n-\frac{1}{2}}\boldsymbol{\lambda}_{n-\frac{1}{2}}$.

For a compact notation, we summarize all nodes $\boldsymbol{x}_n,\ n = 0, ..., N$, resp. all unit quaternions $\boldsymbol{p}_{n-\frac{1}{2}},\ n = 1, ..., N$, in state vectors $\boldsymbol{x}$ and $\boldsymbol{p}$ and write the equations of motion for the discrete Cosserat rod as

$$\begin{pmatrix} m\mathbb{I} & \\ & \boldsymbol{M}(\boldsymbol{p}) \end{pmatrix}\begin{pmatrix} \ddot{\boldsymbol{x}} \\ \ddot{\boldsymbol{p}} \end{pmatrix} = \begin{pmatrix} \boldsymbol{f}^{\boldsymbol{x}}(\boldsymbol{x}, \boldsymbol{p}, \dot{\boldsymbol{x}}, \dot{\boldsymbol{p}}) \\ \boldsymbol{f}^{\boldsymbol{p}}(\boldsymbol{x}, \boldsymbol{p}, \dot{\boldsymbol{x}}, \dot{\boldsymbol{p}}) \end{pmatrix} - \begin{pmatrix} \boldsymbol{0} \\ \boldsymbol{G}_{\boldsymbol{p}}(\boldsymbol{p})^T \end{pmatrix}\boldsymbol{\lambda} \tag{21}$$
$$\boldsymbol{0} = \boldsymbol{g}(\boldsymbol{p})$$

where $\boldsymbol{M}(\boldsymbol{p})$ should be understood as the block-diagonal collection of all quaternion mass matrices, $\boldsymbol{g}(\boldsymbol{p})$ is the collection of all unit quaternion constraints and $\boldsymbol{G}_{\boldsymbol{p}}(\boldsymbol{p})$ the corresponding gradients. Moreover, $\boldsymbol{f}^{\boldsymbol{x}}(\boldsymbol{x}, \boldsymbol{p}, \dot{\boldsymbol{x}}, \dot{\boldsymbol{p}})$ and $\boldsymbol{f}^{\boldsymbol{p}}(\boldsymbol{x}, \boldsymbol{p}, \dot{\boldsymbol{x}}, \dot{\boldsymbol{p}})$ represent all node forces $\boldsymbol{f}^x_n$ and quaternion moments $\boldsymbol{f}^p_{n-\frac{1}{2}}$.

3 LINEAR EQUATIONS OF MOTION

The above system of differential-algebraic equations is non-linear. Before we can compute the mechanical impedance, we need to derive the linearised system, i.e. the corresponding system matrices.

3.1 Linearisation

Let $\left(\tilde{\boldsymbol{x}}^T, \tilde{\boldsymbol{p}}^T, \tilde{\boldsymbol{\lambda}}^T\right)^T$ be the static equilibrium state of the rod for given boundary conditions. Consequently, it holds $\dot{\tilde{\boldsymbol{x}}} = \boldsymbol{0}$ and $\dot{\tilde{\boldsymbol{p}}} = \boldsymbol{0}$ as well as $\ddot{\tilde{\boldsymbol{x}}} = \boldsymbol{0}$ and $\ddot{\tilde{\boldsymbol{p}}} = \boldsymbol{0}$. With perturbations

$\left(\delta\boldsymbol{x}^T, \delta\boldsymbol{p}^T, \delta\boldsymbol{\lambda}^T\right)^T$ we write the disturbed states as

$$\boldsymbol{x} = \tilde{\boldsymbol{x}} + \delta\boldsymbol{x}, \quad \boldsymbol{p} = \tilde{\boldsymbol{p}} + \delta\boldsymbol{p}, \quad \boldsymbol{\lambda} = \tilde{\boldsymbol{\lambda}} + \delta\boldsymbol{\lambda}, \tag{22}$$

$$\dot{\boldsymbol{x}} = \delta\dot{\boldsymbol{x}}, \quad \dot{\boldsymbol{p}} = \delta\dot{\boldsymbol{p}}, \tag{23}$$

$$\ddot{\boldsymbol{x}} = \delta\ddot{\boldsymbol{x}}, \quad \ddot{\boldsymbol{p}} = \delta\ddot{\boldsymbol{p}}. \tag{24}$$

Plugging the disturbed state into the equations of motion (21), we find

$$\begin{aligned}\begin{pmatrix} m\mathbb{I} & \\ & \boldsymbol{M}(\tilde{\boldsymbol{p}}+\delta\boldsymbol{p}) \end{pmatrix} \begin{pmatrix} \delta\ddot{\boldsymbol{x}} \\ \delta\ddot{\boldsymbol{p}} \end{pmatrix} &= \begin{pmatrix} \boldsymbol{f}^{\boldsymbol{x}}(\tilde{\boldsymbol{x}}+\delta\boldsymbol{x}, \tilde{\boldsymbol{p}}+\delta\boldsymbol{p}, \delta\dot{\boldsymbol{x}}, \delta\dot{\boldsymbol{p}}) \\ \boldsymbol{f}^{\boldsymbol{p}}(\tilde{\boldsymbol{x}}+\delta\boldsymbol{x}, \tilde{\boldsymbol{p}}+\delta\boldsymbol{p}, \delta\dot{\boldsymbol{x}}, \delta\dot{\boldsymbol{p}}) \end{pmatrix} - \begin{pmatrix} \boldsymbol{0} \\ \boldsymbol{G}_{\boldsymbol{p}}(\tilde{\boldsymbol{p}}+\delta\boldsymbol{p})^T \end{pmatrix} (\tilde{\boldsymbol{\lambda}}+\delta\boldsymbol{\lambda}) \\ \boldsymbol{0} &= \boldsymbol{g}(\tilde{\boldsymbol{p}}+\delta\boldsymbol{p}) \end{aligned}$$

and the linearisation leads to

$$\begin{aligned}\begin{pmatrix} m\mathbb{I} & \\ & \boldsymbol{M}(\tilde{\boldsymbol{p}}) \end{pmatrix} \begin{pmatrix} \delta\ddot{\boldsymbol{x}} \\ \delta\ddot{\boldsymbol{p}} \end{pmatrix} &= - \begin{pmatrix} \boldsymbol{K}_{\boldsymbol{xx}} & \boldsymbol{K}_{\boldsymbol{xp}} \\ \boldsymbol{K}_{\boldsymbol{px}} & \boldsymbol{K}_{\boldsymbol{pp}} \end{pmatrix} \begin{pmatrix} \delta\boldsymbol{x} \\ \delta\boldsymbol{p} \end{pmatrix} - \begin{pmatrix} \boldsymbol{D}_{\boldsymbol{xx}} & \boldsymbol{D}_{\boldsymbol{xp}} \\ \boldsymbol{D}_{\boldsymbol{px}} & \boldsymbol{D}_{\boldsymbol{pp}} \end{pmatrix} \begin{pmatrix} \delta\dot{\boldsymbol{x}} \\ \delta\dot{\boldsymbol{p}} \end{pmatrix} - \begin{pmatrix} \boldsymbol{0} \\ \boldsymbol{G}_{\boldsymbol{p}}(\tilde{\boldsymbol{p}})^T \end{pmatrix} \delta\boldsymbol{\lambda} \\ \boldsymbol{0} &= \boldsymbol{G}_{\boldsymbol{p}}(\tilde{\boldsymbol{p}})\delta\boldsymbol{p} \end{aligned} \tag{25}$$

with stiffness and damping matrices

$$\begin{pmatrix} \boldsymbol{K}_{\boldsymbol{xx}} & \boldsymbol{K}_{\boldsymbol{xp}} \\ \boldsymbol{K}_{\boldsymbol{px}} & \boldsymbol{K}_{\boldsymbol{pp}} \end{pmatrix} := - \begin{pmatrix} \frac{\partial \boldsymbol{f}^{\boldsymbol{x}}}{\partial \boldsymbol{x}} & \frac{\partial \boldsymbol{f}^{\boldsymbol{x}}}{\partial \boldsymbol{p}} \\ \frac{\partial \boldsymbol{f}^{\boldsymbol{p}}}{\partial \boldsymbol{x}} & \frac{\partial \boldsymbol{f}^{\boldsymbol{p}}}{\partial \boldsymbol{p}} \end{pmatrix}\Bigg|_{(\tilde{\boldsymbol{x}},\tilde{\boldsymbol{p}},\boldsymbol{0},\boldsymbol{0})} + \begin{pmatrix} \boldsymbol{0} & \boldsymbol{0} \\ \boldsymbol{0} & \frac{\partial(\boldsymbol{G}_{\boldsymbol{p}}(\boldsymbol{p})^T\boldsymbol{\lambda})}{\partial \boldsymbol{p}}\Big|_{(\tilde{\boldsymbol{p}},\tilde{\boldsymbol{\lambda}})} \end{pmatrix} \tag{26a}$$

$$\begin{pmatrix} \boldsymbol{D}_{\boldsymbol{xx}} & \boldsymbol{D}_{\boldsymbol{xp}} \\ \boldsymbol{D}_{\boldsymbol{px}} & \boldsymbol{D}_{\boldsymbol{pp}} \end{pmatrix} := - \begin{pmatrix} \frac{\partial \boldsymbol{f}^{\boldsymbol{x}}}{\partial \dot{\boldsymbol{x}}} & \frac{\partial \boldsymbol{f}^{\boldsymbol{x}}}{\partial \dot{\boldsymbol{p}}} \\ \frac{\partial \boldsymbol{f}^{\boldsymbol{p}}}{\partial \dot{\boldsymbol{x}}} & \frac{\partial \boldsymbol{f}^{\boldsymbol{p}}}{\partial \dot{\boldsymbol{p}}} \end{pmatrix}\Bigg|_{(\tilde{\boldsymbol{x}},\tilde{\boldsymbol{p}},\boldsymbol{0},\boldsymbol{0})}. \tag{26b}$$

In principle, the linear system matrices can be computed analytically. However, in our implementation, the linear system matrices are derived by applying algorithmic differentiation. This is done with the C++ library *CoDiPack* [6].

3.2 Transfer to Euclidean moments

Although quaternions are – from our perspective – very attractive to be used, at this particular task the non-regular quaternion mass matrix, the constraint forces due to the unit quaternion constraint and the less-intuitive interpretation is undesired and we prefer the formulation in Euclidean moments. To this end, we use a suitable null space matrix

$$\boldsymbol{T}_{\boldsymbol{p}}(\boldsymbol{p}) = \frac{1}{2} \begin{pmatrix} -p_x & -p_y & -p_z \\ p_s & -p_z & p_y \\ p_z & p_s & -p_x \\ -p_y & p_x & p_s \end{pmatrix} \tag{27}$$

which fulfils $\boldsymbol{G}_{\boldsymbol{p}}\boldsymbol{T}_{\boldsymbol{p}} = \boldsymbol{0}$ and allows to formulate the rotatory equations of motion in minimal coordinates $\delta\boldsymbol{\phi}$. One may recognize, that the columns of $\boldsymbol{T}_{\boldsymbol{p}}(\boldsymbol{p})$ are, up to the factor $\frac{1}{2}$, equal to the last three columns in the quaternion matrix $\boldsymbol{Q}(\boldsymbol{p})$.

We decompose the quaternion perturbations into $\delta\boldsymbol{p} = \boldsymbol{T_p}\delta\boldsymbol{\phi} + \boldsymbol{G_p}^T\boldsymbol{\xi}$, i.e. a tangential and a perpendicular contribution. Next, from $\boldsymbol{0} = \boldsymbol{G_p}\delta\boldsymbol{p} = \boldsymbol{G_p}\boldsymbol{T_p}\delta\boldsymbol{\phi} + \boldsymbol{G_p}\boldsymbol{G_p}^T\boldsymbol{\xi} = \boldsymbol{G_p}\boldsymbol{G_p}^T\boldsymbol{\xi}$, we find $\boldsymbol{\xi} = \boldsymbol{0}$ such that $\delta\boldsymbol{p} = \boldsymbol{T_p}\delta\boldsymbol{\phi}$. Moreover, it holds $\delta\dot{\boldsymbol{p}} = \boldsymbol{T_p}\delta\dot{\boldsymbol{\phi}}$ and $\delta\ddot{\boldsymbol{p}} = \boldsymbol{T_p}\delta\ddot{\boldsymbol{\phi}}$. Plugging this into (25) and left-multiplication with $\boldsymbol{T_p}^T$ yields

$$\begin{aligned}\underbrace{\begin{pmatrix} m\mathbb{I} & \\ & \boldsymbol{T_p}^T\boldsymbol{M}(\tilde{\boldsymbol{p}})\boldsymbol{T_p}\end{pmatrix}}_{=:\boldsymbol{\mathcal{M}}}\begin{pmatrix}\delta\ddot{\boldsymbol{x}}\\ \delta\ddot{\boldsymbol{\phi}}\end{pmatrix} = &-\underbrace{\begin{pmatrix}\boldsymbol{K_{xx}} & \boldsymbol{K_{xp}}\boldsymbol{T_p}\\ \boldsymbol{T_p}^T\boldsymbol{K_{px}} & \boldsymbol{T_p}^T\boldsymbol{K_{pp}}\boldsymbol{T_p}\end{pmatrix}}_{=:\boldsymbol{\mathcal{K}}}\begin{pmatrix}\delta\boldsymbol{x}\\ \delta\boldsymbol{\phi}\end{pmatrix}\\ &-\underbrace{\begin{pmatrix}\boldsymbol{D_{xx}} & \boldsymbol{D_{xp}}\boldsymbol{T_p}\\ \boldsymbol{T_p}^T\boldsymbol{D_{px}} & \boldsymbol{T_p}^T\boldsymbol{D_{pp}}\boldsymbol{T_p}\end{pmatrix}}_{=:\boldsymbol{\mathcal{D}}}\begin{pmatrix}\delta\dot{\boldsymbol{x}}\\ \delta\dot{\boldsymbol{\phi}}\end{pmatrix} - \underbrace{\begin{pmatrix}\boldsymbol{0}\\ \boldsymbol{T_p}^T\boldsymbol{G_p}^T\end{pmatrix}}_{=\boldsymbol{0}}\delta\boldsymbol{\lambda}\\ \boldsymbol{0} = \boldsymbol{G_p}\boldsymbol{T_p}\delta\boldsymbol{\phi} &\equiv \boldsymbol{0}\end{aligned} \tag{28}$$

where constraint forces vanish and the constraint equation is fulfilled per definition. To ease the notation, we introduce a generalized state vector $\boldsymbol{y} = \left(\delta\boldsymbol{x}^T, \delta\boldsymbol{p}^T\right)^T$ and simply write

$$\boldsymbol{\mathcal{M}}\ddot{\boldsymbol{y}} + \boldsymbol{\mathcal{K}}\boldsymbol{y} + \boldsymbol{\mathcal{D}}\dot{\boldsymbol{y}} = \boldsymbol{0}. \tag{29}$$

4 MECHANICAL IMPEDANCE

The equations of motion in the frequency domain, with Fourier-transformed states $\hat{\boldsymbol{y}}(\omega)$, are

$$-\omega^2\boldsymbol{\mathcal{M}}\hat{\boldsymbol{y}}(\omega) + \boldsymbol{\mathcal{K}}\hat{\boldsymbol{y}}(\omega) + i\omega\boldsymbol{\mathcal{D}}\hat{\boldsymbol{y}}(\omega) = \boldsymbol{0}. \tag{30}$$

Here, we introduce structural damping (cf. [7, Ch. 4.8]), we allow a frequency-dependent stiffness matrix $\boldsymbol{\mathcal{K}}(\omega)$ and we assume the viscous damping matrix $\boldsymbol{\mathcal{D}}$ to have several contributions

$$-\omega^2\boldsymbol{\mathcal{M}}\hat{\boldsymbol{y}}(\omega) + (1+i\gamma)\,\boldsymbol{\mathcal{K}}(\omega)\hat{\boldsymbol{y}}(\omega) + i\omega\underbrace{\left(\boldsymbol{\mathcal{D}}_{\mathrm{KV}} + \boldsymbol{\mathcal{D}}_{\mathrm{modal}}\right)}_{=\boldsymbol{\mathcal{D}}}\hat{\boldsymbol{y}}(\omega) = \boldsymbol{0}. \tag{31}$$

The structural damping coefficient γ specifies an additional imaginary stiffness matrix and provides a frequency-independent damping. Supporting $\boldsymbol{\mathcal{K}}(\omega)$ is motivated by possible stiffening effects for larger frequencies. Finally, the generalized viscous damping matrix $\boldsymbol{\mathcal{D}}$ combines $\boldsymbol{\mathcal{D}}_{\mathrm{KV}}$, which results from the linearisation and thus inherits the Kelvin-Voigt type damping, and $\boldsymbol{\mathcal{D}}_{\mathrm{modal}}$. The latter may be constructed, e.g., by Rayleigh damping, modal damping or augmented modal damping (see [7, Ch. 10.3]). All properties are optional and must be set according to the specific application. A more thorough analysis of suitable property options is future work.

To compute the mechanical impedance, we follow [8, Ch. 8.1]. According to the clamping of the rod, we define n_u boundary degrees of freedom $\boldsymbol{u}$ and n_q internal degrees of freedom $\boldsymbol{q}$. Assuming the degrees of freedom are correspondingly rearranged, we can write the equations of motion as

$$\left[-\omega^2\begin{pmatrix}\boldsymbol{\mathcal{M}_{uu}} & \\ & \boldsymbol{\mathcal{M}_{qq}}\end{pmatrix} + (1+i\gamma)\begin{pmatrix}\boldsymbol{\mathcal{K}_{uu}} & \boldsymbol{\mathcal{K}_{uq}}\\ \boldsymbol{\mathcal{K}_{qu}} & \boldsymbol{\mathcal{K}_{qq}}\end{pmatrix} + i\omega\begin{pmatrix}\boldsymbol{\mathcal{D}_{uu}} & \boldsymbol{\mathcal{D}_{uq}}\\ \boldsymbol{\mathcal{D}_{qu}} & \boldsymbol{\mathcal{D}_{qq}}\end{pmatrix}\right]\begin{pmatrix}\hat{\boldsymbol{u}}\\ \hat{\boldsymbol{q}}\end{pmatrix} = \begin{pmatrix}\hat{\boldsymbol{f}}_{\boldsymbol{u}}\\ \boldsymbol{0}\end{pmatrix} \tag{32}$$

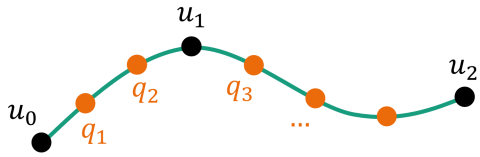

Figure 4: Rod with boundary degrees of freedom $\boldsymbol{u}$ and internal degrees of freedom $\boldsymbol{q}$.

with reaction forces $\hat{\boldsymbol{f}}_{\boldsymbol{u}}$ at the boundary degrees of freedom. For a shorter notation, we summarized the viscous damping again in $\boldsymbol{\mathcal{D}}$ and skipped the frequency-dependence in the state vector, the force vector and the stiffness matrix. From (32) we get the two block equations

$$\hat{\boldsymbol{f}}_{\boldsymbol{u}} = \left[(1+i\gamma)\boldsymbol{\mathcal{K}}_{\boldsymbol{uu}} + i\omega\boldsymbol{\mathcal{D}}_{\boldsymbol{uu}} - \omega^2\boldsymbol{\mathcal{M}}_{\boldsymbol{uu}}\right]\hat{\boldsymbol{u}} + \left[(1+i\gamma)\boldsymbol{\mathcal{K}}_{\boldsymbol{uq}} + i\omega\boldsymbol{\mathcal{D}}_{\boldsymbol{uq}}\right]\hat{\boldsymbol{q}} \tag{33a}$$

$$\boldsymbol{0} = \left[(1+i\gamma)\boldsymbol{\mathcal{K}}_{\boldsymbol{qu}} + i\omega\boldsymbol{\mathcal{D}}_{\boldsymbol{qu}}\right]\hat{\boldsymbol{u}} + \left[(1+i\gamma)\boldsymbol{\mathcal{K}}_{\boldsymbol{qq}} + i\omega\boldsymbol{\mathcal{D}}_{\boldsymbol{qq}} - \omega^2\boldsymbol{\mathcal{M}}_{\boldsymbol{qq}}\right]\hat{\boldsymbol{q}} \tag{33b}$$

where the lower one can be solved for the internal degrees of freedom

$$\hat{\boldsymbol{q}} = -\left[(1+i\gamma)\boldsymbol{\mathcal{K}}_{\boldsymbol{qq}} + i\omega\boldsymbol{\mathcal{D}}_{\boldsymbol{qq}} - \omega^2\boldsymbol{\mathcal{M}}_{\boldsymbol{qq}}\right]^{-1}\left[(1+i\gamma)\boldsymbol{\mathcal{K}}_{\boldsymbol{qu}} + i\omega\boldsymbol{\mathcal{D}}_{\boldsymbol{qu}}\right]\hat{\boldsymbol{u}}. \tag{34}$$

If we plug this into the upper block equation, we get

$$\hat{\boldsymbol{f}}_{\boldsymbol{u}}(\omega) = \boldsymbol{Z}(\omega)\hat{\boldsymbol{u}}(\omega) \tag{35}$$

with impedance matrix $\boldsymbol{Z}(\omega) \in \mathbb{C}^{n_u \times n_u}$ given as

$$\begin{aligned}\boldsymbol{Z}(\omega) = \left[(1+i\gamma)\boldsymbol{\mathcal{K}}_{\boldsymbol{uu}} + i\omega\boldsymbol{\mathcal{D}}_{\boldsymbol{uu}} - \omega^2\boldsymbol{\mathcal{M}}_{\boldsymbol{uu}}\right] - \left[(1+i\gamma)\boldsymbol{\mathcal{K}}_{\boldsymbol{uq}} + i\omega\boldsymbol{\mathcal{D}}_{\boldsymbol{uq}}\right] \\ \cdot\left[(1+i\gamma)\boldsymbol{\mathcal{K}}_{\boldsymbol{qq}} + i\omega\boldsymbol{\mathcal{D}}_{\boldsymbol{qq}} - \omega^2\boldsymbol{\mathcal{M}}_{\boldsymbol{qq}}\right]^{-1}\left[(1+i\gamma)\boldsymbol{\mathcal{K}}_{\boldsymbol{qu}} + i\omega\boldsymbol{\mathcal{D}}_{\boldsymbol{qu}}\right].\end{aligned} \tag{36}$$

Obviously, if the excitation vector $\hat{\boldsymbol{u}}(\omega)$ is known, one can compute the reaction forces $\hat{\boldsymbol{f}}_{\boldsymbol{u}}(\omega) = \boldsymbol{Z}(\omega)\hat{\boldsymbol{u}}(\omega)$ by applying the impedance matrix to the excitation vector. However, often – especially in early virtual development phases – the excitation vector is not available. In this case, one simply investigates the elements of the impedance matrix. Each column of the impedance matrix can be interpreted as the multiplication with the corresponding unit excitation vector. Moreover, each element of the this column represents the transmission of the unit excitation to the corresponding boundary degree of freedom.

5 APPLICATION EXAMPLE

We consider a cooling hose with inner diameter 16mm, wall thickness 3.25 mm, length density $\varrho A = 0.252\,\frac{\text{kg}}{\text{m}}$ and effective stiffness parameters for bending $[EI] = 0.043\,\text{Nm}^2$, torsion $[GJ] = 0.037\,\text{Nm}^2$ and tension $[EA] = 904\,\text{N}$. The effective stiffness parameters are determined with the MeSOMICS measurement system [9]. Moreover, we assume a structural damping with $\gamma = 0.1$, viscous damping is omitted, i.e. $\boldsymbol{\mathcal{D}} = \boldsymbol{0}$, and the stiffness matrix is kept constant, i.e. independent of the frequency.

The hose is clamped at both ends, and we are interested in how the noise transmission from one end A to the other end B is affected by certain modifications. Figure 5 shows the

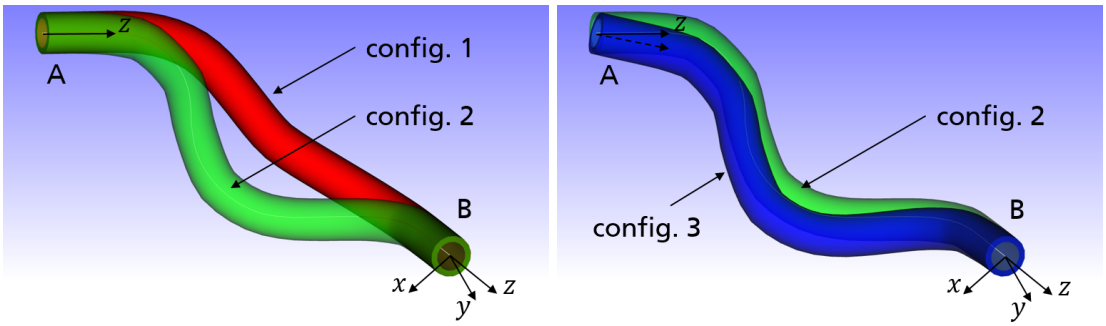

Figure 5: Two hose configurations (config. 1 and config. 2) with different pre-formed shape (*left*) and twice a hose (config. 2 and config. 3) with the same pre-formed shape but slightly tilted boundary condition at A (*right*).

configuration variants we want to analyse. On the left, we show two different pre-formed hose shapes, i.e. different stress-free configurations. On the right, we manipulate the hose at end A by a rotation about 15°.

In principle, excitations in all degrees of freedom (including rotations) can be regarded. Here, we want to apply a longitudinal excitation (in local z-axis) at A and analyse the transmission to B in all directions, i.e. in longitudinal direction (local z-axis) and transversal directions (local x- and y-axis).

In Figure 6, we plot the absolute values of the corresponding entries of the impedance matrix. In longitudinal direction (local z-axis), the first configuration (config. 1) shows the highest noise transmission for approximately 150 Hz, as can be observed from the right plot in Figure 6. For the second configuration (config. 2), the noise transmission at 150 Hz is significantly decreased. However, for the frequency range from 200 Hz to 300 Hz, the impedance is increased. Which configuration is more suitable, of course depends on the application case.

Also worth to mention is that for config. 1 the noise transmission in the local x-axis is larger than in the local y-axis, while for config. 2, this is reversed (see left and middle plot in Figure 6).

Finally, comparing the results for config. 2 and config. 3, only small differences can be observed. Even though config. 3 does not lead to an improved hose assembly, it provides valuable

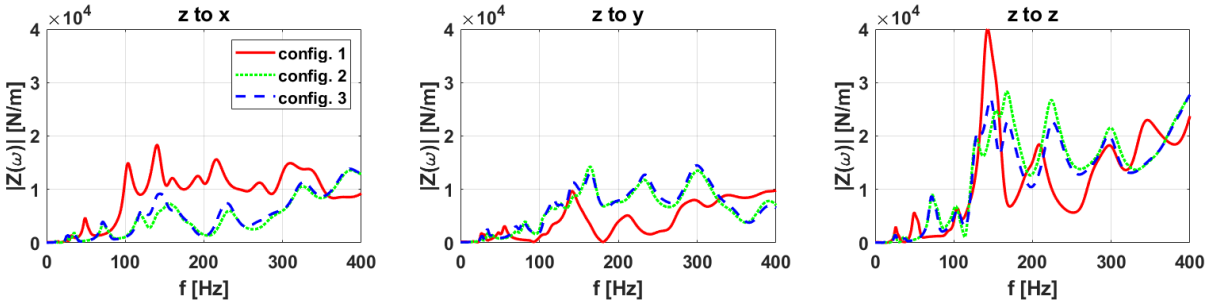

Figure 6: Absolute values of impedance matrix entries for three hose configurations with longitudinal excitation (local z-axis) at A. Plotted is the transmission to B in the local x-axis ("z to x"), the local y-axis ("z to y") and the local z-axis ("z to z").

insights: the applied manipulation of the boundary condition has no negative effect on noise transmission.

6 CONCLUSIONS

We proposed a fast and comfortable methodology for the assessment of noise transmission through highly flexible slender structures like cables and hoses. Starting from interactive simulation with a geometrically exact Cosserat rod, we first derive the linearised equations of motion and use the resulting system matrices to compute the mechanical impedance matrix.

Since the Cosserat rod model enables interactive simulation of cables and hoses and the computation of the mechanical impedance for a static equilibrium of interest is achieved within seconds, the presented approach is very efficient and perfectly suitable to find promising designs for cables and hoses already in the virtual product development.

One open question is how to appropriately specify model parameters like the structural damping coefficient γ or the frequency-dependent stiffness $\boldsymbol{\mathcal{K}}(\omega)$ for real cables or hoses. The latter already arises when identifying the effective stiffness parameters $[EI]$, $[GJ]$ and $[EA]$. Apart from complex measurements, this might be simply impossible due to missing specimens in early development phases. As a consequence, a systematic sensitivity analysis, which helps to understand the importance of the single input quantities, would be desirable.

REFERENCES

[1] Linn, J., Schneider, F., Dreßler, K., Hermanns, O. Virtual Product Development and Digital Validation in Automotive Industry. *In: Bock, H.G., Küfer, KH., Maass, P., Milde, A., Schulz, V. (eds): German Success Stories in Industrial Mathematics. Mathematics in Industry* (2021), vol 35. Springer, Cham.

[2] IPS Cable Simulation Software. *https://flexstructures.com*

[3] Linn, J., Hermansson, T., Andersson, F. and Schneider, F. Kinetic aspects of discrete Cosserat rods based on the difference geometry of framed curves. *Proceedings of the 8th ECCOMAS Thematic Conference on Multibody Dynamics* (2017), pp. 163–175, Prague.

[4] Lang, H., Linn, J. and Arnold, M. Multibody Dynamics Simulation of Geometrically Exact Cosserat Rods. *Multibody System Dynamics* (2011), Vol. **25**(3), pp. 285–312.

[5] Jungkenn, D., Schneider-Jung, F., Andersson, F. and Linn, J. Realistic parameters for dynamic simulation of composite cables using a damped Cosserat rod model. *Proceedings of the 10th ECCOMAS Thematic Conference on Multibody Dynamics* (2019), pp. 391–399, Budapest.

[6] Sagebaum, M., Albring, T. and Gauger, N.R. High-Performance Derivative Computations using CoDiPack. *ACM Transactions on Mathematical Software (TOMS)* (2019), Vol. **45**(4), pp. 1–26.

[7] Craig, R. and Kurdila, A. *Fundamentals of Structural Dynamics.* Wiley (2006).

[8] Géradin, M. and Cardona, A. *Flexible Multibody Dynamics - A Finite Element Approach.* Wiley (2001).

[9] MeSOMICS: Measurement System of the Optically Monitored Identification of Cable Stiffness. *https://www.mesomics.eu*